LLNL-JRNL-2020799

Lawrence Livermore National Laboratory

Alkali Cation Mediated Modulation of CO2 Reduction Activity on Tin Electrodes in EMIM BF4 H2O Electrolytes

B Muchharla, M Gautam, F Nkurunziza, D Ross, S Chatterjee, J Spurgeon, C Hahn, M Janik, B Kumar

Jun 2026

ACS Electrochemistry

This work performed under the auspices of the U.S. Department of Energy by Lawrence Livermore National Laboratory under Contract DE-AC52-07NA27344.

ACS Electrochemistry

pubs.acs.org/electrochem Article

Alkali Cation-Mediated Modulation of CO_2 Reduction Activity on Tin Electrodes in [EMIM][BF_4]/H_2O Electrolytes

Baleeswaraiah Muchharla, Manu Gautam, Francois Nkurunziza, R. Dominic Ross, Soumya Chatterjee, Joshua M. Spurgeon, Christopher Hahn, Michael J. Janik, and Bijandra Kumar*

Cite This: https://doi.org/10.1021/acselectrochem.6c00110 Read Online

ACCESS | Metrics & More | Article Recommendations | Supporting Information

ABSTRACT: The development of efficient CO_2 reduction technologies hinges upon a thorough understanding of the intricate interplay between solution cations and the characteristics of the electrode surface. Recently, ionic liquids (ILs) have emerged as promising electrolytes for the CO_2 reduction reaction. However, the effect of alkali cations on the electrochemical CO_2 reduction (CO_2R) reaction remains unclear in ILs. In this report, we studied alkali cation effects by assessing the electrocatalytic CO_2R activity with the IL 1-ethyl-3-methylimidazolium tetrafluoroborate, [EMIM][BF_4], in water with alkali metal co-cations (i.e., Li^+, Na^+, and K^+) using a polycrystalline Sn catalyst. Contrary to previous findings in purely aqueous media with inorganic cations, where alkali cations strongly enhance CO_2R via pH modulation and strengthening of interfacial electric fields, alkali cations in electrolytes containing the IL [EMIM][BF_4] negatively impact CO_2R activity on Sn electrodes. These results were attributed to the larger radius and higher concentration of the IL organic cation $[EMIM]^+$ that mitigates the impact of alkali cations. These findings highlight the complex interplay between IL cations and alkali metals in shaping CO_2R performance.

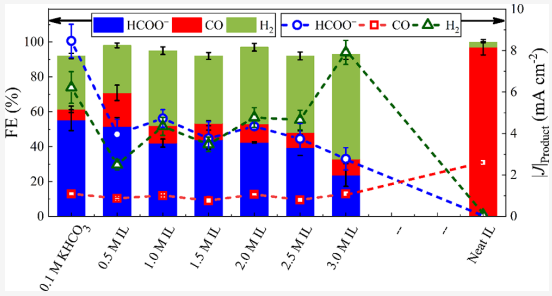

KEYWORDS: *CO_2 electrochemical conversion, ionic liquid, catalysts, cation effect*

INTRODUCTION

As global concerns regarding greenhouse gas emissions and climate change continue to escalate, there is a growing need for efficient and sustainable methods to limit the rise of the atmospheric CO_2 concentration.[1] Electrocatalytic reduction of CO_2 into value-added chemicals is a promising approach to contribute to the mitigation of CO_2 levels in the atmosphere.[2−6] In electrochemical CO_2 reduction (CO_2R), metal catalysts play a crucial role in enhancing the selectivity and efficiency of the process by facilitating the conversion of CO_2 into specific products while minimizing unwanted byproducts.[7−11] Transition metals such as Ag[12−14] and Au[15−17] typically promote the formation of CO, Sn[18−24] promotes the production of $HCOO^-$, and Cu[25−30] is effective in promoting the further reduction of intermediates to hydrocarbon and oxygenate species. Accordingly, product selectivity in CO_2R reflects both the intrinsic properties of the electrode material (which set the preferred surface-bound intermediates) and the electrolyte-controlled interfacial environment (which modulates relative reaction rates through local solvation, proton availability, and double-layer structure).[7,31] In addition to the choice of a catalyst, CO_2R is influenced by the composition of the electrolyte which can help to stabilize reaction intermediates and minimize side reactions, thereby enhancing the efficiency and selectivity of the reduction.[8,32,33]

Recent advances have also highlighted the viability of ionic liquids (ILs) to optimize the reaction energetics and improve overall efficiency.[31] Unlike traditional aqueous electrolytes, ILs offer advantageous properties of low volatility, high ionic conductivity, thermal stability, and a tunable chemical nature. Extensive research on ILs as CO_2R electrolytes has led to several significant review articles[7,31,34−36] and has demonstrated that ILs can alter the CO_2R reaction by directly participating in the reaction mechanism.[37,38] A Ag cathode in [EMIM][BF_4] can convert CO_2 to CO at overpotentials less than 0.2 V,[39] which was attributed to the IL cation lowering the energy of the CO_2 intermediate (e.g., CO_2^-) by forming a complex that subsequently decreases the activation energy for reduction.[39,40] Imidazolium cations can act as proton donors, forming neutral EMIM−CO_2 adducts instead of generating negatively charged species like OH^- or HCO_3^-, which would

Received: March 16, 2026
Revised: May 18, 2026
Accepted: June 15, 2026

otherwise accumulate and weaken the interfacial electric field. By maintaining a cation-rich interface and avoiding co-ion buildup, the electric double layer remains thin, sustaining strong local electric fields that stabilize key intermediates and create a favorable microenvironment for CO_2R.[41] Taken together, prior studies suggest that imidazolium cations such as $[EMIM]^+$ can facilitate CO_2R through multiple, not mutually exclusive, roles: (i) stabilizing CO_2-derived intermediates via specific interactions and/or complexation, thereby lowering the barrier for the initial CO_2 activation step; (ii) restructuring the electrical double layer to maintain a cation-rich interfacial region and strong local electric fields that further stabilize polar intermediates; and (iii) modulating the balance between CO_2R and HER in a manner that depends on electrode material and the IL/H_2O ratio.[39,42,43] These effects have been established most clearly on Ag and Au electrodes in imidazolium-based ILs and IL/H_2O mixtures.[39,42,44]

The presence of alkali metal cations in the electrolyte is also known to influence the CO_2R process.[45−48] In conventional aqueous media, the faradaic efficiency of CO_2R products is highly dependent on the identity of the alkali cations. Larger cations, such as Cs^+, typically lead to enhanced CO_2R current density in water compared to smaller cations, following the activity trend $Li^+ < Na^+ < K^+ < Rb^+ < Cs^+$.[49−51] This phenomenon is attributed to the accumulation of charged cations at the outer Helmholtz plane, where they stabilize reaction intermediates through electrostatic interactions and modulate the interfacial electric field.[46,52] The smaller cations have a higher charge density and more strongly attract water, leading to a larger hydration shell that limits how densely the cations can pack at the electrode interface. The varying interfacial electrocatalyst environment among electrolytes significantly alters the activity and selectivity for conversion of CO_2 into desired products such as CO, $HCOO^-$, or hydrocarbons, which depend on the specific reaction conditions and the catalyst used. However, when alkali cations are introduced into IL-containing electrolytes like $[EMIM][BF_4]$, the interactions among ions and solvent at the electrode interface become more complex and are even less understood.[53] Unlike aqueous electrolytes, where alkali effects might be interpreted as heuristically derived from variations in average electric fields[46,54] or direct stabilization of intermediates,[50,55,56] ILs bring additional complicating factors. For example, the formation of reactive intermediates, such as carbene species,[57,58] and charge-neutral $EMIM-CO_2$ adducts[42,59] can influence the reaction environment and CO_2R pathways in imidazolium-based ILs. The (unknown) partitioning of IL or alkali ions in the interfacial region, dependent on electrolyte composition and operating potential, further complicates interpretation of their observed effects on CO_2R activity and selectivity. Optimizing CO_2R in ILs and in mixed complex electrolytes may require different strategies from those employed in aqueous media, particularly concerning electrolyte composition and ion-pairing effects.[35] Thus, while the influence of alkali metal cations on CO_2R in aqueous systems is well documented,[49,52] it remains unclear how these effects translate to IL-based systems such as $[EMIM][BF_4]$.

In imidazolium-based IL electrolytes, much of what is known about electrolyte-driven enhancements has been established on Ag and Au surfaces, where $[EMIM]^+$ can restructure the electrical double layer and stabilize CO_2-derived intermediates and where the IL/H_2O ratio can strongly tune activity and suppress HER under certain conditions.[39,42,44] In contrast, the specific role of added alkali cations in these IL/H_2O environments is far less established than in purely aqueous electrolytes.[43,60] Unlike in water, where alkali-cation identity is often explained by how strongly cations hydrate and how they shape the electric field near the electrode, IL/H_2O mixtures with both organic and alkali cations add extra complexity, such as ion pairing, which ions actually reach the interface, and competition between ions that can change the interface and reaction pathways in catalyst-dependent ways.[46,51] Consequently, a clear mechanistic picture of how alkali cations influence CO_2R in imidazolium IL/H_2O mixtures, and whether aqueous "alkali promotion" trends persist, remains an open question.

Our recent work[43] demonstrated that while imidazolium-based ILs and alkali cations independently enhance CO_2R activity on Ag surfaces, their combined presence leads to inhibition effects due to competition for adsorption sites at the electrode−electrolyte interface. During CO_2R on Ag, alkali cations, particularly Li^+, can hinder imidazolium-mediated catalysis by disrupting the electric double layer, probably by competing with $[EMIM]^+$ for adsorption sites and preventing the reorientation of $[EMIM]^+$ at the electrode surface.[43] Unlike Ag and Au, which predominantly reduce CO_2 to CO via *COOH/*CO intermediates, Sn-based electrodes favor the formation of formate through a distinct OCHO* intermediate.[18,61] This mechanistic preference arises from the comparatively stronger interaction of Sn with oxygen-bound species, which stabilizes bidentate, oxygen-coordinated intermediates relative to carbon-bound *COOH species. As a result, CO formation on Sn is kinetically disfavored, while the OCHO* pathway to $HCOO^-$ becomes dominant under aqueous conditions. These fundamental differences in intermediate stabilization and transition-state energetics mean that the same electrolyte environment can lead to qualitatively different selectivity trends on Sn versus Ag or Au. This mechanistic difference suggests that the role of alkali cations in IL−based CO_2R on Sn could diverge significantly from their effect on Ag, highlighting the need for dedicated studies in such systems.[62,63]

In this study, we address this gap by systematically investigating CO_2R on a polycrystalline Sn foil electrode in a mixed $[EMIM][BF_4]/H_2O$ electrolytes, with and without added alkali cations. This work builds directly on prior IL/H_2O studies largely concentrated on Ag and on our recent demonstration that alkali cations can inhibit imidazolium-mediated CO formation on Ag, by extending the mixed-cation question to Sn, a mechanistically distinct catalyst that predominantly proceeds through an OCHO* intermediate to formate.[43] Specifically, we focus on two key aspects: (1) the effect of varying $[EMIM][BF_4]$ concentrations on CO_2 conversion activity and product distribution in comparison to purely aqueous electrolyte conditions and (2) the impact of different alkali metal cations within the $[EMIM][BF_4]/H_2O$ matrix on CO_2R performance. The insights gained will elucidate how IL-based electrolyte composition and cation identity collectively govern CO_2R pathways on Sn, providing a mechanistic basis for designing electrolyte−catalyst combinations optimized for selective and efficient product formation.

MATERIALS AND METHODS

Chemicals and Materials

Potassium bicarbonate ($KHCO_3$, 99.95%), lithium tetrafluoroborate ($LiBF_4$, 98%), sodium tetrafluoroborate ($NaBF_4$, 98%), potassium tetrafluoroborate (KBF_4, 99.99%), and 1-ethyl-3-methylimidazolium

https://doi.org/10.1021/acselectrochem.6c00110
ACS Electrochem. XXXX, XXX, XXX−XXX

tetrafluoroborate [EMIM][BF_4] (≥98%) were purchased from Millipore Corp. Tin foil (Sn, 0.127 mm thickness, 99.9%, Sigma Aldrich) was cleaned by smoothening of the surface through sequential abrasion with 600 grit and 800 grit sandpapers to eliminate surface irregularities and enhance uniformity. The Sn foil was then sonicated in ethanol for 5 min to remove any residual contaminants. Following this, the Sn foil was meticulously rinsed with deionized water to ensure the removal of any remaining solvent and impurities. To prevent oxidation and maintain the treated surface integrity, the Sn foil was dried under a stream of N_2 gas.

Electrochemical Measurements

All electrochemical experiments were conducted in a gastight, low volume electrochemical H-cell with a Nafion N117 membrane used as a separator between the anode and cathode chambers. Electrochemical characterizations were performed using a BioLogic potentiostat SP-300. In this study, cleaned Sn foil was used as the working electrode, Pt mesh was the counter electrode, and Ag/AgCl saturated in KCl was the reference electrode. All reported voltage data was adjusted by 85% iR correction to account for the uncompensated series resistance using a resistance determined by electrochemical impedance spectroscopy measurements prior to each experiment. All potentials were converted to the RHE scale by

$$E_{RHE} = E_{Ag/AgCl} + 0.197\ \text{V} + 0.0592^{*}\text{pH}$$

The pH values of all electrolytes were measured before and after CO_2 purging, as detailed in Tables S1 and S2. CO_2 reduction reaction kinetics were studied with linear sweep voltammetry (LSV) measurements by sweeping the potential between 0.0 V and −1.2 V vs RHE at a scan rate of 20 mV s^{-1}. Constant potential electrolysis (CPE) was performed at −0.9 V, −1.0 V, −1.1 V, and −1.2 V vs RHE under continuous CO_2 bubbling at 10 sccm.

Product Analysis

The gas phase products were quantified using a gas chromatograph (GC) (SRI Instruments, Model 8610C) equipped with both a thermal conductivity detector (TCD) and a flame ionization detector (FID). The GC sampled 1 mL at an exhaust flow rate of 10 sccm after 20 min during the CPE. At the end of each reaction, the liquid products were analyzed by ^{1}H NMR spectroscopy (Agilent V NMRS 700 MHz). NMR samples were prepared by adding 600 μL of electrolyte solution and 200 μL of d_6 DMSO (Cambridge Isotopes, 99.9%) containing a DMF internal standard having a known concentration. The samples were then analyzed in an NMR spectroscope equipped with an HCN cryoprobe using a two-signal solvent suppression pulse sequence. The integration values of $HCOO^-$ (chemical shift, δ ∼ 8.3 ppm, Figure S1) were measured against the DMF internal standard. For both gas and liquid products, faradaic efficiency (FE) was computed by assessing the charge necessary to generate the observed product concentration and then dividing by the total charge passed throughout the electrolysis time to generate the sample.

RESULTS

LSVs were acquired using a Sn foil working electrode immersed in an electrolyte with varied concentrations of [EMIM][BF_4] IL dissolved in water, and the results were compared with CO_2R performed in 0.1 M $KHCO_3$ aqueous solution under similar experimental conditions (Figure 1 and Figure S2). In IL-based electrolytes, an increase in current density was evident in the presence of CO_2-bubbled (30 min) electrolytes (Figure 1A). In the absence of CO_2, the current density reached only −4 mA cm^{-2} at the most negative applied potential (−1.2 V vs RHE) tested. This comparatively small CO_2-free current provides an upper bound on background processes (e.g., HER and any minor non-CO_2R reductions) under our operating conditions, indicating that the substantially larger currents measured under CO_2 are predominantly associated with CO_2R and HER competition rather than other side reactions. Upon introducing CO_2, a substantial enhancement in current density was observed, reaching −13.5 mA cm^{-2} at a similar potential in 0.5 M [EMIM][BF_4], indicating a strong contribution from CO_2R processes. A similar trend was observed in all electrolytes except 0.1 M $KHCO_3$ solution (Figure S2). The total current density increased with increasing IL molarity and reached a maximum current density with 2.0 M IL before decreasing again at 3.0 M IL (Figure 1B). The inset in Figure 1B provides a zoomed-in view in the range of the onset potential. This behavior is consistent with prior observations on Ag electrodes in similar experimental conditions,[43,60] where intermediate [EMIM][BF_4] concentrations maximize CO_2 reduction activity due to optimal double-layer structuring, while higher IL concentrations reduce performance because of increased viscosity and diminished mass transport.

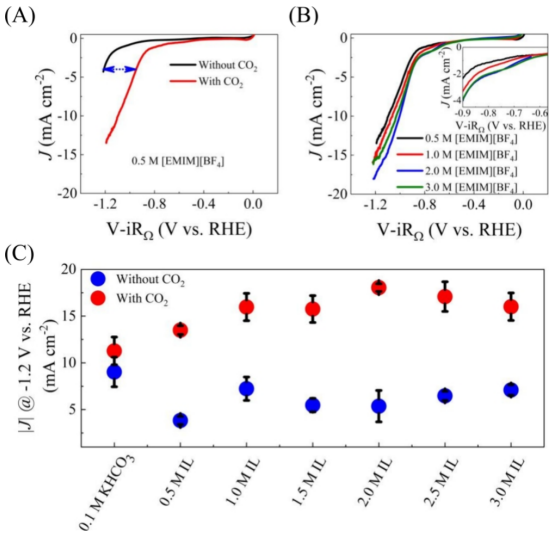

Figure 1. Effect of [EMIM][BF_4] concentration on the current density vs potential behavior. (A) LSVs of Sn foil in 0.5 M [EMIM][BF_4] electrolyte with and without CO_2 bubbling. The dotted blue line with arrows indicates the potentials at a current density of −4 mA cm^{-2}. (B) LSVs of Sn foil in CO_2-saturated electrolyte with varying concentrations of [EMIM][BF_4]. The inset shows a zoomed-in view. (C) Total current density at an applied potential of −1.2 V vs RHE vs [EMIM][BF_4] concentration. The error bars represent the standard deviation from at least three independent measurements.

CPE measurements were conducted at different potentials (i.e., −0.9, −1.0, −1.1 and −1.2 V vs RHE) to analyze the CO_2R gaseous and liquid product distribution as a function of IL concentrations (Figure S3). After an initial transient, the system reached a steady state, and a nearly constant current density was sustained for 40 min at each applied potential (Figure S3). Figure 2A shows the FEs for the evolved products at different potentials in CO_2-saturated 2.0 M [EMIM][BF_4]. The FE for $HCOO^-$ increased from 29.5% at −0.9 V to 42.5% at −1.2 V vs RHE, while the FE for CO decreased from 31.6% at −0.9 V to 11.0% at −1.2 V vs RHE. Simultaneously,

https://doi.org/10.1021/acselectrochem.6c00110
ACS Electrochem. XXXX, XXX, XXX–XXX

the FE for H_2 increased from 36% at −0.9 V to 44% at −1.2 V vs RHE. Corresponding FE versus potential data for all electrolyte compositions, shown in Figure S4, further illustrates how the relative formation of $HCOO^-$, CO, and H_2 evolves with both IL concentration and applied potential. The influence of [EMIM][BF_4] concentration on the competition between CO_2 reduction and hydrogen evolution was evaluated by plotting the ratio of carbon-based partial current densities ($HCOO^-$ + CO) to the H_2 partial current density (J_{C_1}/J_{H_2}) as a function of applied potential (Figure 2B). At low IL concentration (0.5 M), the J_{C_1}/J_{H_2} ratio increases at higher negative potentials, indicating improved selectivity toward carbon products relative to H_2. In contrast, at higher IL concentrations (≥1.0 M), the ratio slightly decreases at higher negative potentials (≤−1.0 V vs RHE), suggesting a diminished ability of the electrolyte to suppress HER. More broadly, the trend in product distribution with potential was observed to shift with [EMIM][BF_4] concentration (Figure 2B and Figure S5). For the lowest tested IL concentrations, 0.1 M $KHCO_3$ (0 M IL) and 0.5 M [EMIM][BF_4], a larger fraction of carbon-based products was formed at increasingly cathodic potentials. In contrast, the fraction of carbon-based products decreased at more negative potentials for the highest IL concentrations (>2.0 M [EMIM][BF_4]). The intermediate concentrations of 1.0 M and 1.5 M [EMIM][BF_4] marked a transition between these trends with the maximum ratio of carbon product to hydrogen formation occurring in the middle of this potential range.

Figure 2C shows a comparison of FEs and partial current densities for H_2, CO, and $HCOO^-$ with varying [EMIM][BF_4] concentration at −1.2 V vs RHE. The FE for $HCOO^-$ decreased with increasing IL concentration, with a notable drop from 56% FE in the absence of IL to 24% FE with 3.0 M [EMIM][BF_4] and further decreased to 0% FE with neat IL, 6.54 M [EMIM][BF_4] (Figure 2C). However, within the range of 1.0−2.5 M [EMIM][BF_4], the FE for $HCOO^-$ remained relatively constant at 40%. Despite varying the [EMIM][BF_4] concentration, no clear trend was observed in the CO faradaic efficiency across the mixed IL−water electrolytes, indicating that CO formation on Sn remains a minor pathway under these conditions. Specifically, a FE of 19% for CO was recorded in CO_2-saturated 0.5 M [EMIM][BF_4], while within the concentration range of 1.0−3.0 M [EMIM][BF_4], the FE for CO remained relatively stable at ∼10%. However, a pronounced increase in CO production with an FE of ∼97% for CO was observed in neat IL. Because the Sn electrode and operating protocol are held constant across these measurements, this large shift in selectivity with IL/H_2O composition indicates that the $[EMIM]^+$-rich interfacial microenvironment can substantially reorganize the double layer and solvation structure, thereby redirecting CO_2R/HER competition and product distributions even on the same catalyst surface. The strong CO signal in neat IL therefore reflects a shift in interfacial solvation and proton activity unique to the water-free ionic liquid environment. This behavior suggests that the highly non-aqueous interfacial environment of pure [EMIM][BF_4] fundamentally alters the reaction pathway, likely by stabilizing CO_2^- or *COOH intermediates and suppressing proton availability, thereby favoring the CO route over the $HCOO^-$ pathway typically dominant on Sn in aqueous or partially hydrated systems. The FE for H_2 from the HER increased from 30% in the absence of IL to 60% at 3.0 M [EMIM][BF_4] and then plummeted to only 3% in neat IL. The partial current

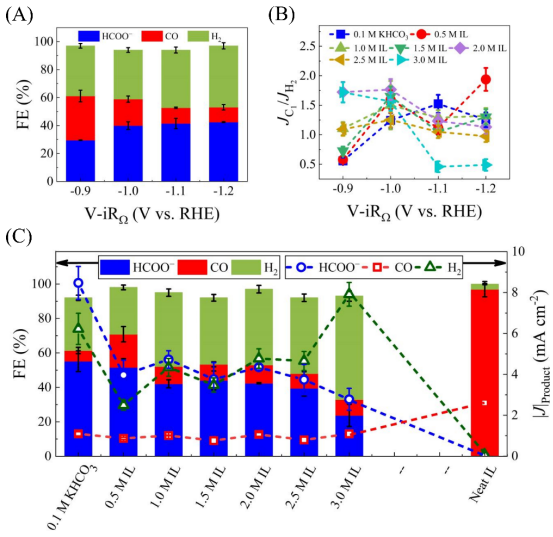

Figure 2. Effect of [EMIM][BF_4] concentration in water on CO_2R on a Sn foil cathode. (A) FE vs potential in CO_2-saturated 2.0 M [EMIM][BF_4]. (B) Ratio of partial current densities for C_1 products to H_2 as a function of potential across all IL concentrations. (C) Comparison of FE and partial current density vs [EMIM][BF_4] concentration at −1.2 V vs RHE. The error bars represent the standard deviation from at least three independent measurements.

density of ∼8.5 mA cm^{-2} was observed for $HCOO^-$ without any IL, but the value decreased steadily with increasing IL concentration to only 2.8 mA cm^{-2} with 3.0 M [EMIM][BF_4]. A steady CO partial current density of ∼1.0 mA cm^{-2} was observed as the IL concentration increased to 3.0 M; a further increase to neat IL led to an enhanced CO partial current density of 2.6 mA cm^{-2}. The partial current density for H_2 was about 7.6 mA cm^{-2} without any IL. At a concentration of 0.5 M [EMIM][BF_4], the partial current density for H_2 was observed to be about 2.5 mA cm^{-2}, which further increased to 7.9 mA cm^{-2} at 3.0 M [EMIM][BF_4].

Having determined the concentration window in which the IL impacts CO_2R, we continued by investigating how adding alkali cations further shapes the observed activity and selectivity trends. To investigate the impact of alkali cations in the IL [EMIM][BF_4] on CO_2R on Sn, electrolytes of [EMIM][BF_4]/H_2O with different alkali cations were used, as illustrated in Figure 3A. To maintain a constant total cation concentration, salts with monovalent alkali cations of varied ionic radii (Li^+, Na^+, and K^+, Table S3) were maintained at 0.1 M with 1.9 M [EMIM][BF_4], which were compared to results with 2.0 M [EMIM][BF_4] in the absence of alkali salts. A 2.0 M IL concentration was chosen because it led to the highest current density (Figure 1B). Alkali tetrafluoroborate salts were used to prevent convoluting effects that might be attributable to different anions. The LSV data indicates that increasing alkali cation size correlates with an enhanced total current density, in agreement with CO_2R trends observed for alkali salts in purely aqueous solutions.[50−53] In the absence of alkali cations, a current density of around −18 mA cm^{-2} was observed at an applied potential of −1.2 V vs RHE. Upon substituting 0.1 M

https://doi.org/10.1021/acselectrochem.6c00110
ACS Electrochem. XXXX, XXX, XXX−XXX

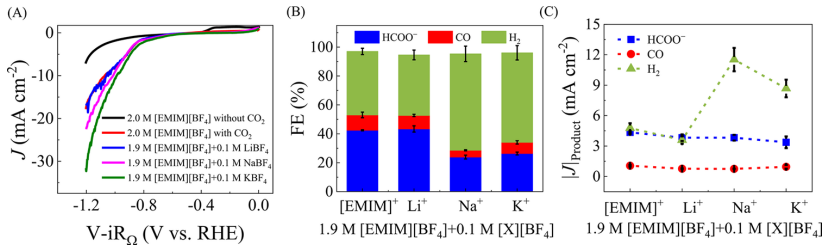

Figure 3. Effect of varying alkali cations in IL [EMIM][BF_4] on CO_2R. (A) LSV curves for a Sn cathode in 1.9 M [EMIM][BF_4] with 0.1 M [X][BF_4] added, all under CO_2 bubbling except the black curve. (B) FE of evolved products in the presence of different cations at an applied potential of −1.2 V vs RHE. (C) Partial current density comparison of H_2, CO, and $HCOO^-$ with varying cations at an applied potential of −1.2 V vs RHE. The error bars represent the standard deviation from at least three independent measurements.

$[EMIM]^+$ with K^+ ions in the electrolyte, the current density increased to around −32 mA cm^{-2}.

Figure 3B shows the product distributions at −1.2 V vs RHE with different alkali cations. CPE measurements for all electrolyte conditions, 1.9 M [EMIM][BF_4] + 0.1 M [X][BF_4] (X = EMIM, Li, Na, or K), at different potentials (i.e., −0.9, −1.0, −1.1, and −1.2 V vs RHE) are displayed in Figure S6. Though the presence of Li^+ had little effect on selectivity at these conditions, both Na^+ and K^+ promoted HER at the expense of $HCOO^-$ selectivity (Figure 3B, Figure S7). A FE of 42.5% for $HCOO^-$ was measured in 2.0 M IL, which increased slightly to 43.4% upon the substitution of 0.1 M Li^+. However, the FE for $HCOO^-$ decreased to ∼25% using Na^+ or K^+ cations. Conversely, the FE for CO did not exhibit a clear trend with increasing cation mass. The 44% H_2 FE measured in 2.0 M [EMIM][BF_4] was mostly unaffected with the presence of Li^+ but increased significantly with Na^+ and K^+ to as high as 67% FE, suggesting a strong promotion of HER from these alkali cations at this potential.

Figure 3C illustrates the product partial current densities with varying alkali cations. While the $HCOO^-$ FE decreased appreciably for the larger alkali cations, the concomitant increase in total current density partially offsets this decrease, with a partial current density for $HCOO^-$ dropping from 4.35 mA cm^{-2} for 2.0 M [EMIM][BF_4] at −1.2 V vs RHE to 3.37 mA cm^{-2} when substituting in 0.1 M KBF_4. The smaller CO partial current density was mostly unaffected by the presence of the alkali cations. Following the H_2 FE trend, the hydrogen partial current density of 4.77 mA cm^{-2} in 2.0 M [EMIM][BF_4] was only modestly affected in the presence of Li^+ but increased significantly to 11.52 mA cm^{-2} using Na^+ and to 8.68 mA cm^{-2} with K^+ cations. Notably, although Na^+/K^+ increases the total current density, the product-resolved partial current densities show that this increase is dominated by H_2 formation, while CO partial currents change little and $HCOO^-$ partial currents decrease modestly (Figure 3C). These product-resolved trends indicate that the additional current induced by Na^+ or K^+ primarily reflects preferential promotion of HER under these mixed-cation IL/H_2O conditions.

For all electrolyte conditions, 1.9 M [EMIM][BF_4] + 0.1 M [X][BF_4] (X = EMIM, Li, Na, or K), the partial current density for $HCOO^-$ generally increased with more negative applied potential (Figure 4). The CO partial current density showed little variation across applied potentials for all electrolytes. The partial current density for H_2 was similar to the behavior for $HCOO^-$ in 2.0 M [EMIM][BF_4] without alkali cations.

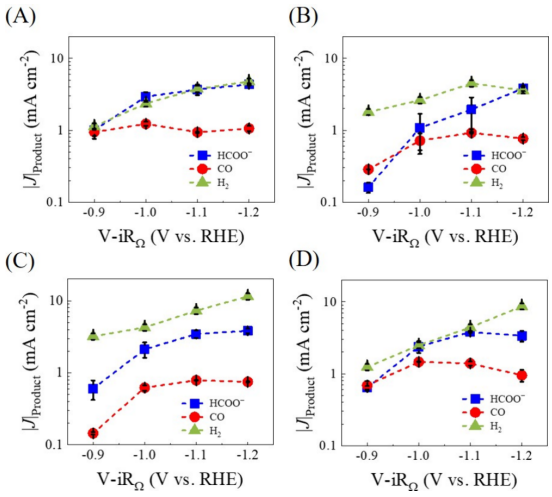

Figure 4. Effect of [EMIM][BF_4] concentration on CO_2R on a Sn foil cathode. The partial current density vs potential using (A) 2.0 M [EMIM][BF_4], (B) 1.9 M [EMIM][BF_4] + 0.1 M $LiBF_4$, (C) 1.9 M [EMIM][BF_4] + 0.1 M $NaBF_4$, and (D) 1.9 M [EMIM][BF_4] + 0.1 M KBF_4. The error bars represent the standard deviation from at least three independent measurements.

However, in the presence of 0.1 M Li^+, the H_2 partial current density was higher before decreasing at −1.2 V vs RHE. Most notably, with 0.1 M of either Na^+ or K^+ cations, the applied potential significantly impacted the H_2 partial current density, increasing in value 2−3× from −0.9 V to −1.2 V vs RHE. The sharp increase in hydrogen production with Na^+ or K^+ at more cathodic potentials with little corresponding change for $HCOO^-$ or CO suggests that these cations play a role in promoting HER preferentially over CO_2R on Sn.

DISCUSSION

A central point of context for interpreting selectivity trends is that product distributions in CO_2R arise from both catalyst identity and electrolyte composition. The electrode material sets the baseline preference for key intermediates (e.g., Sn favoring the OCHO* pathway to formate under aqueous conditions), whereas the electrolyte tunes the interfacial

https://doi.org/10.1021/acselectrochem.6c00110
ACS Electrochem. XXXX, XXX, XXX−XXX

microenvironment (solvation structure, proton activity/availability, and double-layer organization) and thereby shifts the relative rates of CO_2R pathways versus HER. Since we use the same polycrystalline Sn foil electrode throughout and systematically vary only the electrolyte composition (IL/H_2O ratio and added alkali cations), the selectivity changes discussed below primarily reflect electrolyte-driven modulation of the interfacial environment on a fixed catalyst.

The IL concentration has a significant effect on CO_2R on Sn by impacting both the total current density and the product distribution. The trend with an intermediate IL concentration leading to peak current density is similar to concentration effects previously observed for ILs with Ag, in which more concentrated ILs thin the EDL through more free cations at the interface until a critical threshold in IL concentration where ion-pairing leads to neutral aggregates that decrease reaction rates due to consequently greater screening lengths.[60] In purely aqueous electrolyte with Sn, $HCOO^-$ was the dominant product, consistent with the established OCHO* pathway for Sn-based catalysts.[18,61] For Sn in an imidazolium-based IL in water, we observed that increasing [EMIM][BF_4] concentration progressively decreased the FE for $HCOO^-$ while promoting hydrogen evolution, with CO remaining a minor product (Figure 2). This trend may suggest that at higher IL concentrations, the increasingly dominant $[EMIM]^+$ environment restructures the interfacial region in a way that disfavors the OCHO* intermediate, possibly by altering local solvation or proton availability needed for $HCOO^-$ formation. We note this only as a hypothesis, as direct spectroscopic evidence would be required to confirm such interfacial changes. A growing body of work demonstrates that the balance of ionic liquid and water is a key factor in tuning CO_2R selectivity, though the effect depends strongly on the catalyst. Rosen et al. reported that Ag electrodes in [EMIM][BF_4]/H_2O mixtures achieved nearly 100% FE for CO at ∼90 mol % water, with HER strongly suppressed.[64] To place these conditions in the context of the present study, ∼90 mol % water corresponds approximately to ∼10 mol % [EMIM][BF_4], or ∼3.0 M [EMIM][BF_4] assuming ideal mixing and commonly reported IL densities. This concentration range overlaps closely with the higher [EMIM][BF_4] concentrations examined here (e.g., 3.0 M [EMIM][BF_4]), where a markedly different selectivity behavior is observed on Sn. In contrast to Ag,[43] Sn electrodes in the present work exhibit substantial HER at comparable IL/H_2O ratios and do not display a composition window in which CO_2R proceeds with near-unity CO selectivity. This divergence underscores the catalyst-dependent nature of imidazolium-based electrolyte effects. While $EMIM^+$-rich environments can suppress HER and stabilize CO_2-derived intermediates on Ag, favoring *COOH/*CO pathways, the same electrolyte compositions on Sn, which primarily proceeds through an OCHO* (formate) pathway in aqueous media, lead to enhanced proton availability and competitive HER. These results highlight that electrolyte composition effects established on Ag cannot be directly translated to mechanistically distinct catalysts such as Sn without accounting for differences in reaction pathways and surface−electrolyte interactions. Similarly, Zhu et al. showed that Ag, Au, and Pd all exhibit high CO selectivity in IL/H_2O mixtures, with intermediate water concentration giving the best performance due to a synergy between proton availability from $[BF_4]^-$ hydrolysis and HER suppression by $[EMIM]^+$ adsorption.[65] Taken together, these comparisons underscore the central novelty of the present study: in mixed [EMIM][BF_4]/H_2O electrolytes, alkali cations do not universally "promote CO_2R" but instead exert strongly catalyst-dependent effects, and on Sn, they primarily increase HER rather than enhancing the formate pathway.

During conventional CO_2R in purely aqueous electrolyte, changes in the interfacial pK_a as a function of increasing alkali cation size is reported to lower the interfacial electric field, leading to increased availability of interfacial CO_2.[66] As the nominal cation radius becomes larger, the effective cation hydration radius concurrently decreases due to the lower charge density and leads to a lower cation-electrode surface separation and thus stronger electric field effects.[66] These effects are also generalizable to other electrocatalytic reactions, in which the accumulation of charge at the outer Helmholtz plane (OHP) is increased with smaller solvated cation size. More cations and thus higher charge density at the OHP lead to enhanced stabilization of polarizable adsorbates by creating a less diffuse EDL. Thus, on Sn in purely aqueous electrolyte, both $HCOO^-$ and CO production rates increase with nominal alkali cation size while HER is largely unaffected due to the lack of a dipole moment for adsorbed *H.[52]

In contrast, enhanced CO_2R on Sn was not observed with 0.1 M Li^+, Na^+, or K^+ alkali cations in 1.9 M [EMIM][BF_4] (Figure 3). Unlike the Sn behavior with alkali cations in purely aqueous solvent, a large increase in the HER rate was measured with Na^+ and K^+ in solutions of imidazolium−based IL despite the lack of a dipole moment for adsorbed *H.[52] While minor unquantified side reactions cannot be fully excluded in concentrated IL-containing electrolytes, the product-resolved partial currents show that the dominant change upon introducing Na^+ and K^+ is increased H_2 formation, indicating that HER accounts for most of the additional cathodic current under these conditions. Simultaneously, the partial current density for CO remained steady in the presence of alkali cations while that for $HCOO^-$ modestly decreased with increasing nominal alkali cation size (Figure 3C), both in contrast to the reported behavior for Sn with alkalis in purely aqueous conditions. Thus, it is clear that the interaction of alkali and $[EMIM]^+$ cations inhibits the CO_2R promotional effect of alkali cations observed in the absence of IL. The presence of Li^+ led to little difference in performance compared to the [EMIM][BF_4] alone aside from a small decrease in the rate of $HCOO^-$ formation. One possible explanation is that the interface becomes highly enriched in $[EMIM]^+$ at these IL concentrations, and this dense layer of organic cations may restrict the ability of strongly hydrated species such as Li^+ to approach the electrode. With limited interfacial access, a substantial fraction of Li^+ would interact weakly with the EDL and therefore have only a minor influence on the imidazolium-mediated CO_2R pathway. In contrast, Na^+ and K^+, with smaller hydration shells, might be blocked less in migrating through the IL ions to play a role in the EDL. This interpretation is still consistent with the observed trend in overall current density, in which larger alkali cations (e.g., Na^+ and K^+) with overall smaller hydration shells lead to stronger total current density (Figure 3A). Protonated water molecules that are shuttled to the electrode interface through the alkali cation hydration spheres likely increase the interfacial water concentration in the IL solution and thus enable more proton donors for HER. Consistent with the product-resolved analysis, Na^+ and K^+ increase the H_2 partial current density substantially relative to the IL-only electrolyte

https://doi.org/10.1021/acselectrochem.6c00110
ACS Electrochem. XXXX, XXX, XXX−XXX

(Figures 3B,C and 4). We therefore propose as a working hypothesis that alkali cations with smaller hydration shells (Na^+/K^+) may access the interfacial region more effectively in the presence of $[EMIM]^+$, thereby modifying interfacial solvation and water availability in a way that favors HER; however, confirming hydration-shell-mediated proton delivery or changes in interfacial water activity will require direct interfacial probes. In the presence of alkali cations, electrocatalysis on Sn seems to proceed without significantly affecting the imidazolium-mediated mechanism for CO_2R, in which the CO_2 coordinates with the $EMIM^+$ at an active site and $HCOO^-$ production consequently may not benefit from proton availability in the hydration shells of alkali cations at other surface sites.

The gradual deactivation of CO_2R on Sn in $[EMIM][BF_4]$ with increasing alkali cation size, as exhibited by moderately decreased $HCOO^-$ partial current density (Figure 3C), indicates that the alkalis have an inhibitory effect on imidazolium-mediated $HCOO^-$ production in addition to degrading the selectivity through HER promotion. The reasons for the inhibition of $HCOO^-$ production may include competitive adsorption between alkali cations and $[EMIM]^+$ at active sites as well as alkali cations impeding the reorientation of $[EMIM]^+$ at the surface under applied potential, both factors that were found to contribute to the inhibitory effect of alkali cations in imidazolium-mediated CO_2R on Ag.[43] Possibly, the presence of alkali cations could also disrupt the ordering of IL ions in the EDL and the role of entropy in promoting CO_2R by imidazolium cations.[44] Overall, however, the relatively minor effect of alkali cations on CO_2R at the cathode surface is partly attributable to the much higher concentration and larger size of the organic $[EMIM]^+$ cations, leading to them dominating the double layer behavior and product distribution compared to that observed with alkali cations in purely aqueous electrolyte on Sn.[52]

Notably, some of the results herein deviated from trends observed in recent work on CO_2R on Ag in imidazolium IL with alkali cations, which reported a sharp inhibition of CO formation on Ag in the presence of alkali cations, especially with Li^+.[43] Our data on Sn electrodes exhibited only a modest decline in $HCOO^-$ selectivity and partial current density with alkali cations, with the least effect caused by Li^+, and with no significant effect on CO formation. This difference suggests that the competition between $[EMIM]^+$ and alkali cations at the electrode surface manifests differently on Sn than on Ag, possibly due to the different binding energy of Sn which results in its stronger affinity for the $HCOO^-$ conversion pathway. These observations underscore the importance of catalyst-specific interfacial interactions in mixed-cation environments.

We also performed density functional theory (DFT) calculations to examine the competition for specific adsorption of Li^+, Na^+, and $[EMIM]^+$ at a Sn(200) surface, contrasting with prior work examining specific adsorption to the Ag(111) surface.[43] DFT results (Figure S8, with accompanying method details) suggest Li^+ outcompetes $[EMIM]^+$ for the Sn(200)surface at cathodic potentials relevant to CO_2R. Li^+ adsorbs more favorably to Sn(200) than to Ag(111) whereas $[EMIM]^+$ adsorption is equivalent to the two surfaces. These results do not support the hypothesis based on experimental results that the minor effects of Li^+ on CO_2R on Sn are due to a low affinity of Li^+ for the near-surface region. This disagreement may be more indicative of limitations in the use of a single Sn (200) surface and reduced representation of the complex electrode−IL interface in the DFT model than refuting the hypothesized interfacial behavior. Stronger mechanistic insights and evidence may be achievable through in situ spectroscopic investigations such as surface-enhanced Raman spectroscopy (SERS) to unravel the distinction in behavior between Ag vs Sn in mixed alkali/EMIM electrolytes. However, the relative inactivity of Sn surfaces for SERS presents a challenge and may require a more sophisticated method such as shell-isolated nanoparticle-enhanced Raman spectroscopy (SHINERS).[67]

CONCLUSIONS

In advancing electrochemical CO_2 reduction technologies, it is imperative to comprehend the underlying mechanisms governing cation effects at the electrode surface. The CO_2R behavior of Sn, an exemplar catalyst favoring the $HCOO^-$ production pathway, was investigated in a mixed $[EMIM][BF_4]/H_2O$ electrolyte with and without added alkali salts to examine the role of mixed cation interactions. Without alkali cations, increased $[EMIM][BF_4]$ concentration led to generally decreased rates of $HCOO^-$ production. With alkali cations (0.1 M Li^+, Na^+, or K^+) added to 1.9 M $[EMIM][BF_4]$, the heavier alkali cations induced higher total current density but not a concomitant enhancement of CO_2R, contrary to findings from analogous studies conducted with alkali cations in purely aqueous electrolyte. Alkali cations detrimentally affected CO_2R on Sn in $[EMIM][BF_4]/H_2O$ by enhancing HER, possibly through water in their hydration shell promoting/participating in HER and by inhibiting C1 (CO, $HCOO^-$) product formation through interference with any imidazolium-mediated pathways. Alkali cations detrimentally affected CO_2R selectivity on Sn in $[EMIM][BF_4]/H_2O$ primarily by increasing the H_2 partial current density (most strongly for Na^+ and K^+), while CO partial currents were comparatively unchanged and $HCOO^-$ partial currents decreased modestly under the same conditions. Based on these product-resolved trends, we attribute the higher total cathodic currents in Na^+/K^+-containing electrolytes predominantly to preferential promotion of HER. We further note as a working hypothesis that cation-associated water and/or alkali-imidazolium competition within the interfacial double layer may contribute to this HER promotion and the modest suppression of $HCOO^-$ formation; direct validation will require future in situ interfacial spectroscopy and kinetic probes. These findings suggest that optimizing IL composition and minimizing competing cation interactions help achieve selective and efficient CO_2R in IL−based electrolytes. Future investigations should build greater understanding of the complex interaction between cation types (e.g., organic and alkali) and electrocatalytic processes at the cathode/electrolyte interface, thereby laying the groundwork for informed electrolyte design principles in advancing next-generation CO_2 reduction technologies. Additional in situ experiments (e.g., SHINERS, dynamic electrochemical impedance spectroscopy, etc.) combined with theoretical modeling will be essential to elucidate the mechanisms by which alkali cations interact with ILs and affect the behavior on Sn differently from other surfaces.

ASSOCIATED CONTENT

Supporting Information

The Supporting Information is available free of charge at https://pubs.acs.org/doi/10.1021/acselectrochem.6c00110.

https://doi.org/10.1021/acselectrochem.6c00110
ACS Electrochem. XXXX, XXX, XXX−XXX

Additional experimental details, NMR spectra, and computational details (DOCX)

AUTHOR INFORMATION

Corresponding Author

Bijandra Kumar – *Department of Mathematics, Computer Science and Engineering Technology, Elizabeth City State University, Elizabeth City, North Carolina 27909, United States*; orcid.org/0000-0002-7985-5903; Email: bkumar@ecsu.edu

Authors

Baleeswaraiah Muchharla – *Department of Mathematics, Computer Science and Engineering Technology, Elizabeth City State University, Elizabeth City, North Carolina 27909, United States*

Manu Gautam – *Conn Center for Renewable Energy Research, University of Louisville, Louisville, Kentucky 40292, United States*

Francois Nkurunziza – *Conn Center for Renewable Energy Research, University of Louisville, Louisville, Kentucky 40292, United States*

R. Dominic Ross – *Materials Science Division, Lawrence Livermore National Laboratory, Livermore, California 94550, United States*; orcid.org/0000-0002-4192-8230

Soumya Chatterjee – *Department of Chemical Engineering, The Pennsylvania State University, State College, University Park, Pennsylvania 16802, United States*

Joshua M. Spurgeon – *Conn Center for Renewable Energy Research, University of Louisville, Louisville, Kentucky 40292, United States*; orcid.org/0000-0002-2987-0865

Christopher Hahn – *Materials Science Division, Lawrence Livermore National Laboratory, Livermore, California 94550, United States*; orcid.org/0000-0002-2772-6341

Michael J. Janik – *Department of Chemical Engineering, The Pennsylvania State University, State College, University Park, Pennsylvania 16802, United States*

Complete contact information is available at: https://pubs.acs.org/doi/10.1021/acselectrochem.6c00110

Notes

The authors declare no competing financial interest.

ACKNOWLEDGMENTS

Research was primarily supported as part of the Center for Closing the Carbon Cycle, an Energy Frontier Research Center funded by the U.S. Department of Energy (DOE), Office of Science, Basic Energy Sciences (BES), under Award Number DE−SC0023427. Work by R.D.R. and C.H. was conducted under the auspices of the U.S. Department of Energy by Lawrence Livermore National Laboratory under Contract DE-AC52-07NA27344.

REFERENCES

(1) Zickfeld, K.; MacIsaac, A. J.; Canadell, J. G.; Fuss, S.; Jackson, R. B.; Jones, C. D.; Lohila, A.; Matthews, H. D.; Peters, G. P.; Rogelj, J.; Zaehle, S. Net-zero approaches must consider Earth system impacts to achieve climate goals. *Nat. Clim. Change.* **2023**, *13* (12), 1298−1305.

(2) Nielsen, D. U.; Hu, X.-M.; Daasbjerg, K.; Skrydstrup, T. Chemically and electrochemically catalysed conversion of CO_2 to CO with follow-up utilization to value-added chemicals. *Nat. Catal.* **2018**, *1* (4), 244−254.

(3) Quan, Y.; Zhu, J.; Zheng, G. Electrocatalytic Reactions for Converting CO_2 to Value-Added Products. *Small Sci.* **2021**, *1* (10), No. 2100043.

(4) Wang, G.; Chen, J.; Ding, Y.; Cai, P.; Yi, L.; Li, Y.; Tu, C.; Hou, Y.; Wen, Z.; Dai, L. Electrocatalysis for CO_2 conversion: from fundamentals to value-added products. *Chem. Soc. Rev.* **2021**, *50* (8), 4993−5061.

(5) Wu, J.; Sharifi, T.; Gao, Y.; Zhang, T.; Ajayan, P. M. Emerging Carbon-Based Heterogeneous Catalysts for Electrochemical Reduction of Carbon Dioxide into Value-Added Chemicals. *Adv. Mater.* **2019**, *31* (13), No. 1804257.

(6) Kumar, B.; Muchharla, B.; Dikshit, M.; Dongare, S.; Kumar, K.; Gurkan, B.; Spurgeon, J. M. Electrochemical CO_2 Conversion Commercialization Pathways: A Concise Review on Experimental Frontiers and Technoeconomic Analysis. *Environ. Sci. Technol. Lett.* **2024**, *11* (11), 1161-1174.

(7) Kumar, B.; Brian, J. P.; Atla, V.; Kumari, S.; Bertram, K. A.; White, R. T.; Spurgeon, J. M. New trends in the development of heterogeneous catalysts for electrochemical CO_2 reduction. *Catal. Today* **2016**, *270*, 19−30.

(8) Franco, F.; Rettenmaier, C.; Jeon, H. S.; Roldan Cuenya, B. Transition metal-based catalysts for the electrochemical CO_2 reduction: from atoms and molecules to nanostructured materials. *Chem. Soc. Rev.* **2020**, *49* (19), 6884−6946.

(9) Han, J.; Bai, X.; Xu, X.; Bai, X.; Husile, A.; Zhang, S.; Qi, L.; Guan, J. Advances and challenges in the electrochemical reduction of carbon dioxide. *Chem. Sci.* **2024**, *15* (21), 7870−7907.

(10) Guo, L.; Zhou, J.; Liu, F.; Meng, X.; Ma, Y.; Hao, F.; Xiong, Y.; Fan, Z. Electronic Structure Design of Transition Metal-Based Catalysts for Electrochemical Carbon Dioxide Reduction. *ACS Nano* **2024**, *18* (14), 9823−9851.

(11) Leonzio, G.; Hankin, A.; Shah, N. CO_2 electrochemical reduction: A state-of-the-art review with economic and environmental analyses. *Chem. Eng. Res. Des.* **2024**, *208*, 934−955.

(12) Dongare, S.; Coskun, O. K.; Cagli, E.; Lee, K. Y. C.; Rao, G.; Britt, R. D.; Berben, L. A.; Gurkan, B. A Bifunctional Ionic Liquid for Capture and Electrochemical Conversion of CO_2 to CO over Silver. *ACS Catal.* **2023**, *13* (12), 7812−7821.

(13) Yoon, Y.; Hall, A. S.; Surendranath, Y. Tuning of Silver Catalyst Mesostructure Promotes Selective Carbon Dioxide Conversion into Fuels. *Angew. Chem., Int. Ed.* **2016**, *55* (49), 15282−15286.

(14) Quan, F.; Xiong, M.; Jia, F.; Zhang, L. Efficient electroreduction of CO_2 on bulk silver electrode in aqueous solution via the inhibition of hydrogen evolution. *Appl. Surf. Sci.* **2017**, *399*, 48−54.

(15) Cai, X.; Li, G.; Hu, W.; Zhu, Y. Catalytic Conversion of CO_2 over Atomically Precise Gold-Based Cluster Catalysts. *ACS Catal.* **2022**, *12* (17), 10638−10653.

(16) Zhang, B. A.; Costentin, C.; Nocera, D. G. On the Conversion Efficiency of CO_2 Electroreduction on Gold. *Joule* **2019**, *3* (7), 1565−1568.

(17) Nursanto, E. B.; Jeon, H. S.; Kim, C.; Jee, M. S.; Koh, J. H.; Hwang, Y. J.; Min, B. K. Gold catalyst reactivity for CO_2 electro-reduction: From nano particle to layer. *Catal. Today* **2016**, *260*, 107−111.

(18) Naikkath, A.; Mohan, N. G.; Ramanujam, K.; Srinivasan, R. Mechanism of electrochemical carbon dioxide reduction to formate on tin electrode. *Chem. Eng. J.* **2024**, *482*, No. 148972.

(19) Bienen, F.; Kopljar, D.; Geiger, S.; Wagner, N.; Friedrich, K. A. Investigation of CO_2 Electrolysis on Tin Foil by Electrochemical Impedance Spectroscopy. *ACS Sustainable Chem. Eng.* **2020**, *8* (13), 5192−5199.

(20) Fan, T.; Zhang, J.; Zhang, X.; Wang, M.; Yi, X.; Lum, Y.; Chen, Z. Interface-stabilized high-valent Sn enables efficient CO_2 electroreduction to formate/formic acid across the full pH range. *Nano Energy* **2024**, *130*, No. 110135.

(21) Zhang, S.; Kang, P.; Meyer, T. J. Nanostructured Tin Catalysts for Selective Electrochemical Reduction of Carbon Dioxide to Formate. *J. Am. Chem. Soc.* **2014**, *136* (5), 1734−1737.

(22) Liu, H.; Miao, B.; Chuai, H.; Chen, X.; Zhang, S.; Ma, X. Nanoporous tin oxides for efficient electrochemical CO_2 reduction to formate. *Green Chem. Eng.* **2022**, *3* (2), 138−145.
(23) Kumar, B.; Atla, V.; Brian, J. P.; Kumari, S.; Nguyen, T. Q.; Sunkara, M.; Spurgeon, J. M. Reduced SnO_2 Porous Nanowires with a High Density of Grain Boundaries as Catalysts for Efficient Electrochemical CO_2-into-HCOOH Conversion. *Angew. Chem., Int. Ed.* **2017**, *56* (13), 3645−3649.
(24) Rao, K. R.; Pishgar, S.; Strain, J.; Kumar, B.; Atla, V.; Kumari, S.; Spurgeon, J. M. Photoelectrochemical reduction of CO_2 to HCOOH on silicon photocathodes with reduced SnO_2 porous nanowire catalysts. *J. Mater. Chem. A* **2018**, *6* (4), 1736−1742.
(25) Amirbeigiarab, R.; Tian, J.; Herzog, A.; Qiu, C.; Bergmann, A.; Roldan Cuenya, B.; Magnussen, O. M. Atomic-scale surface restructuring of copper electrodes under CO_2 electroreduction conditions. *Nat. Catal.* **2023**, *6* (9), 837−846.
(26) Dai, Y.; Li, H.; Wang, C.; Xue, W.; Zhang, M.; Zhao, D.; Xue, J.; Li, J.; Luo, L.; Liu, C.; Li, X.; Cui, P.; Jiang, Q.; Zheng, T.; Gu, S.; Zhang, Y.; Xiao, J.; Xia, C.; Zeng, J. Manipulating local coordination of copper single atom catalyst enables efficient CO_2-to-CH_4 conversion. *Nat. Commun.* **2023**, *14* (1), No. 3382.
(27) Jun, M.; Kundu, J.; Kim, D. H.; Kim, M.; Kim, D.; Lee, K.; Choi, S.-I. Strategies to Modulate the Copper Oxidation State Toward Selective C_{2+} Production in the Electrochemical CO_2 Reduction Reaction. *Adv. Mater.* **2024**, *36* (21), No. 2313028.
(28) Wang, X.; Ju, W.; Liang, L.; Riyaz, M.; Bagger, A.; Filippi, M.; Rossmeisl, J.; Strasser, P. Electrochemical CO_2 Activation and Valorization on Metallic Copper and Carbon-Embedded N-Coordinated Single Metal MNC Catalysts. *Angew. Chem., Int. Ed. Engl.* **2024**, *63* (21), No. e202401821.
(29) Tabassum, H.; Yang, X.; Zou, R.; Wu, G. Surface engineering of Cu catalysts for electrochemical reduction of CO_2 to value-added multicarbon products. *Chem Catalysis* **2022**, *2* (7), 1561−1593.
(30) Fan, Q.; Zhang, M.; Jia, M.; Liu, S.; Qiu, J.; Sun, Z. Electrochemical CO_2 reduction to C_{2+} species: Heterogeneous electrocatalysts, reaction pathways, and optimization strategies. *Mater. Today Energy* **2018**, *10*, 280−301.
(31) Dongare, S.; Zeeshan, M.; Aydogdu, A. S.; Dikki, R.; Kurtoğlu-Öztulum, S. F.; Coskun, O. K.; Muñoz, M.; Banerjee, A.; Gautam, M.; Ross, R. D.; Stanley, J. S.; Brower, R. S.; Muchharla, B.; Sacci, R. L.; Velázquez, J. M.; Kumar, B.; Yang, J. Y.; Hahn, C.; Keskin, S.; Morales-Guio, C. G.; Uzun, A.; Spurgeon, J. M.; Gurkan, B. Reactive capture and electrochemical conversion of CO_2 with ionic liquids and deep eutectic solvents. *Chem. Soc. Rev.* **2024**, *53* (17), 8563−8631.
(32) O'Brien, C. P.; Miao, R. K.; Shayesteh Zeraati, A.; Lee, G.; Sargent, E. H.; Sinton, D. CO_2 Electrolyzers. *Chem. Rev.* **2024**, *124* (7), 3648−3693.
(33) Pei, Y. ; Zhong, H. ; Jin, F. A brief review of electrocatalytic reduction of CO_2—Materials, reaction conditions, and devices. **2021**, *9* (7), 1012-1032.
(34) Li, Y.; Li, F.; Laaksonen, A.; Wang, C.; Cobden, P.; Boden, P.; Liu, Y.; Zhang, X.; Ji, X. Electrochemical CO_2 reduction with ionic liquids: review and evaluation. *Ind. Chem. Mater.* **2023**, *1* (3), 410−430.
(35) An, X.; Wang, P.; Ma, X.; Du, X.; Hao, X.; Yang, Z.; Guan, G. Application of ionic liquids in CO_2 capture and electrochemical reduction: A review. *Carbon Resour. Convers.* **2023**, *6* (2), 85−97.
(36) Lv, H.; Dai, C.; Xu, R.; Wang, N.; Chen, B.; Yu, G. In−depth understanding on the mechanism of ionic liquid-assisted enhancement of electrochemical CO_2 reduction to formic acid. *Int. J. Hydrogen. Energy* **2024**, *104*, 103.
(37) Asadi, M.; Kim, K.; Liu, C.; Addepalli, A. V.; Abbasi, P.; Yasaei, P.; Phillips, P.; Behranginia, A.; Cerrato, J. M.; Haasch, R.; Zapol, P.; Kumar, B.; Klie, R. F.; Abiade, J.; Curtiss, L. A.; Salehi-Khojin, A. Nanostructured transition metal dichalcogenide electrocatalysts for CO_2 reduction in ionic liquid. *Science* **2016**, *353* (6298), 467-470.
(38) Asadi, M.; Kumar, B.; Behranginia, A.; Rosen, B. A.; Baskin, A.; Repnin, N.; Pisasale, D.; Phillips, P.; Zhu, W.; Haasch, R.; Klie, R. F.; Král, P.; Abiade, J.; Salehi-Khojin, A. Robust carbon dioxide reduction on molybdenum disulphide edges. *Nat. Commun.* **2014**, *5* (1), No. 4470.
(39) Rosen, B. A.; Salehi-Khojin, A.; Thorson, M. R.; Zhu, W.; Whipple, D. T.; Kenis, P. J. A.; Masel, R. I. Ionic Liquid–Mediated Selective Conversion of CO_2 to CO at Low Overpotentials. *Science* **2011**, *334* (6056), 643−644.
(40) Motobayashi, K.; Maeno, Y.; Ikeda, K. In Situ Spectroscopic Characterization of an Intermediate of CO_2 Electroreduction on a Au Electrode in Room-Temperature Ionic Liquids. *J. Phys. Chem. C* **2022**, *126* (29), 11981−11986.
(41) Guo, W.; Liu, B.; Gebbie, M. A. Suppressing Co-Ion Generation via Cationic Proton Donors to Amplify Driving Forces for Electrochemical CO_2 Reduction. *J. Phys. Chem. C* **2023**, *127* (29), 14243−14254.
(42) Neyrizi, S.; Kiewiet, J.; Hempenius, M. A.; Mul, G. What It Takes for Imidazolium Cations to Promote Electrochemical Reduction of CO_2. *ACS Energy Lett.* **2022**, *7* (10), 3439−3446.
(43) Nkurunziza, F.; Dongare, S.; Chatterjee, S.; Shah, B.; Gautam, M.; Muchharla, B.; Kumar, B.; Janik, M. J.; Gurkan, B.; Sacci, R. L.; Spurgeon, J. M. Alkali Cation Inhibition of Imidazolium-Mediated Electrochemical CO_2 Reduction on Silver. *J. Am. Chem. Soc.* **2025**, *147* (9), 7564−7577.
(44) Noh, S.; Cho, Y. J.; Zhang, G.; Schreier, M. Insight into the Role of Entropy in Promoting Electrochemical CO_2 Reduction by Imidazolium Cations. *J. Am. Chem. Soc.* **2023**, *145* (50), 27657−27663.
(45) Yang, X.; Ding, H.; Li, S.; Zheng, S.; Li, J.-F.; Pan, F. Cation-Induced Interfacial Hydrophobic Microenvironment Promotes the C−C Coupling in Electrochemical CO_2 Reduction. *J. Am. Chem. Soc.* **2024**, *146* (8), 5532−5542.
(46) Ringe, S.; Clark, E. L.; Resasco, J.; Walton, A.; Seger, B.; Bell, A. T.; Chan, K. Understanding cation effects in electrochemical CO_2 reduction. *Energy. Environ. Sci.* **2019**, *12* (10), 3001−3014.
(47) Zhong, X.; Peng, H.-J.; Xia, C.; Liu, X. Electrolyte Effect on Electrochemical CO_2 Reduction to Multicarbon Products. *J. Phys. Chem. C* **2024**, *128* (9), 3621−3631.
(48) Pan, B.; Wang, Y.; Li, Y. Understanding and leveraging the effect of cations in the electrical double layer for electrochemical CO_2 reduction. *Chem Catal.* **2022**, *2* (6), 1267−1276.
(49) Malkani, A. S.; Anibal, J.; Xu, B. Cation Effect on Interfacial CO_2 Concentration in the Electrochemical CO_2 Reduction Reaction. *ACS Catal.* **2020**, *10* (24), 14871−14876.
(50) Monteiro, M. C. O.; Dattila, F.; López, N.; Koper, M. T. M. The Role of Cation Acidity on the Competition between Hydrogen Evolution and CO_2 Reduction on Gold Electrodes. *J. Am. Chem. Soc.* **2022**, *144* (4), 1589−1602.
(51) Ovalle, V. J.; Hsu, Y.-S.; Agrawal, N.; Janik, M. J.; Waegele, M. M. Correlating hydration free energy and specific adsorption of alkali metal cations during CO_2 electroreduction on Au. *Nat. Catal.* **2022**, *5* (7), 624−632.
(52) Resasco, J.; Chen, L. D.; Clark, E.; Tsai, C.; Hahn, C.; Jaramillo, T. F.; Chan, K.; Bell, A. T. Promoter Effects of Alkali Metal Cations on the Electrochemical Reduction of Carbon Dioxide. *J. Am. Chem. Soc.* **2017**, *139* (32), 11277−11287.
(53) Moura de Salles Pupo, M.; Kortlever, R. Electrolyte Effects on the Electrochemical Reduction of CO_2. *ChemPhysChem* **2019**, *20* (22), 2926−2935.
(54) Gu, J.; Liu, S.; Ni, W.; Ren, W.; Haussener, S.; Hu, X. Modulating electric field distribution by alkali cations for CO_2 electroreduction in strongly acidic medium. *Nat. Catal.* **2022**, *5* (4), 268−276.
(55) Shin, S.-J.; Choi, H.; Ringe, S.; Won, D. H.; Oh, H.-S.; Kim, D. H.; Lee, T.; Nam, D.-H.; Kim, H.; Choi, C. H. A unifying mechanism for cation effect modulating C1 and C2 productions from CO_2 electroreduction. *Nat. Commun.* **2022**, *13* (1), No. 5482.
(56) Oh, S.; Morales-Collazo, O.; Keller, A. N.; Brennecke, J. F. Cation−Anion and Anion−CO_2 Interactions in Triethyl(octyl)phosphonium Ionic Liquids with Aprotic Heterocyclic Anions (AHAs). *J. Phys. Chem. B* **2020**, *124* (40), 8877−8887.

https://doi.org/10.1021/acselectrochem.6c00110
ACS Electrochem. XXXX, XXX, XXX–XXX

(57) Gurau, G.; Rodríguez, H.; Kelley, S. P.; Janiczek, P.; Kalb, R. S.; Rogers, R. D. Demonstration of Chemisorption of Carbon Dioxide in 1,3-Dialkylimidazolium Acetate Ionic Liquids. **2011**, *50* (50), 12024−12026.
(58) Gohndrone, T. R.; Song, T.; DeSilva, M. A.; Brennecke, J. F. Quantification of Ylide Formation in Phosphonium-Based Ionic Liquids Reacted with CO_2. *J. Phys. Chem. B* **2021**, *125* (24), 6649−6657.
(59) Mei, K.; He, X.; Chen, K.; Zhou, X.; Li, H.; Wang, C. Highly Efficient CO_2 Capture by Imidazolium Ionic Liquids through a Reduction in the Formation of the Carbene−CO_2 Complex. *Ind. Eng. Chem. Res.* **2017**, *56* (28), 8066−8072.
(60) Liu, B.; Guo, W.; Gebbie, M. A. Tuning Ionic Screening To Accelerate Electrochemical CO_2 Reduction in Ionic Liquid Electrolytes. *ACS Catal.* **2022**, *12* (15), 9706−9716.
(61) Whittaker, T. N.; Fishler, Y.; Clary, J. M.; Brimley, P.; Holewinski, A.; Musgrave, C. B.; Farberow, C. A.; Smith, W. A.; Vigil-Fowler, D. Insights into Electrochemical CO_2 Reduction on Metallic and Oxidized Tin Using Grand-Canonical DFT and In Situ ATR-SEIRA Spectroscopy. *ACS Catal.* **2024**, *14* (11), 8353−8365.
(62) Boutin, E.; Haussener, S. Rate-Determining Step for Electrochemical Reduction of Carbon Dioxide into Carbon Monoxide at Silver Electrodes. *ACS Catal.* **2024**, *14* (11), 8437−8445.
(63) Tricella, C.; Muhyuddin, M.; Nisticò, R.; Tosoni, S.; Santoro, C. Recent advancements related to silver-based electrocatalysts for carbon dioxide reduction reaction to carbon monoxide. *Curr. Opin. Electrochem.* **2025**, *51*, No. 101696.
(64) Rosen, B. A.; Zhu, W.; Kaul, G.; Salehi-Khojin, A.; Masel, R. I. Water Enhancement of CO_2 Conversion on Silver in 1-Ethyl-3-Methylimidazolium Tetrafluoroborate. *J. Electrochem. Soc.* **2013**, *160* (2), H138.
(65) Feaster, J. T.; Jongerius, A. L.; Liu, X.; Urushihara, M.; Nitopi, S. A.; Hahn, C.; Chan, K.; Nørskov, J. K.; Jaramillo, T. F. Understanding the Influence of [EMIM]Cl on the Suppression of the Hydrogen Evolution Reaction on Transition Metal Electrodes. *Langmuir* **2017**, *33* (37), 9464−9471.
(66) Singh, M. R.; Kwon, Y.; Lum, Y.; Ager, J. W., III; Bell, A. T. Hydrolysis of Electrolyte Cations Enhances the Electrochemical Reduction of CO_2 over Ag and Cu. *J. Am. Chem. Soc.* **2016**, *138* (39), 13006−13012.
(67) Li, J. F.; Huang, Y. F.; Ding, Y.; Yang, Z. L.; Li, S. B.; Zhou, X. S.; Fan, F. R.; Zhang, W.; Zhou, Z. Y.; Wu, D. Y.; Ren, B.; Wang, Z. L.; Tian, Z. Q. Shell-isolated nanoparticle-enhanced Raman spectroscopy. *Nature* **2010**, *464* (7287), 392−395.

https://doi.org/10.1021/acselectrochem.6c00110
ACS Electrochem. XXXX, XXX, XXX−XXX